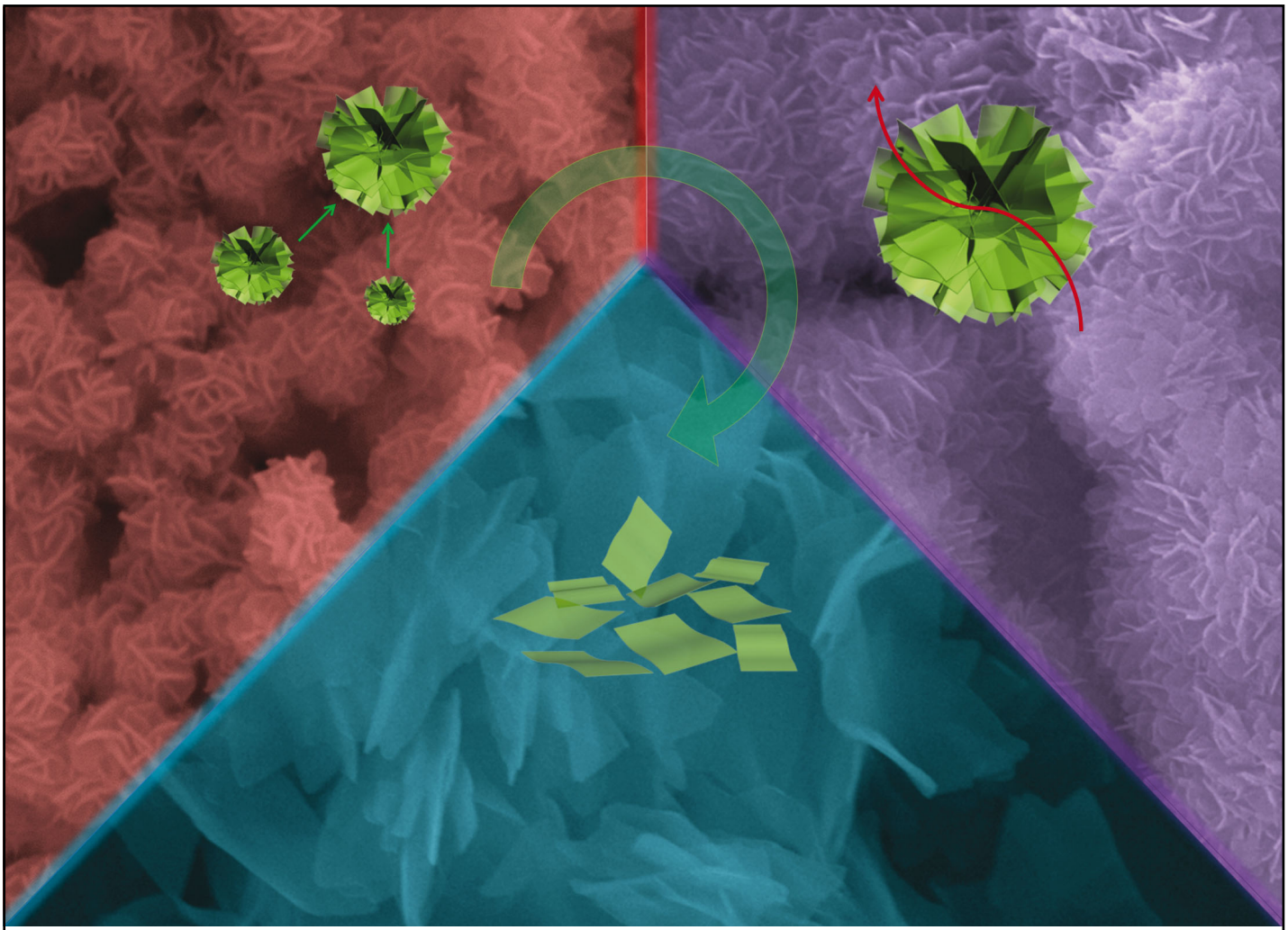

Showcasing research work from the Liqiang Mai group, State Key Laboratory of Advanced Technology for Materials Synthesis and Processing, WUT-Harvard Joint Nano Key Laboratory, Wuhan University of Technology.

Title: Supercritically exfoliated ultrathin vanadium pentoxide nanosheets with high rate capability for lithium batteries

A novel supercritical solvothermal method is successfully established to synthesize the exfoliated ultrathin vanadium pentoxide nanosheets, which exhibit outstanding high-rate capability due to the shortened diffusion distance and increased electrode–electrolyte contact area.

As featured in:

See Mai *et al.*, *Phys. Chem. Chem. Phys.*, 2013, **15**, 16828.

www.rsc.org/pccp

Registered Charity Number 207890

PCCP

RSC Publishing

PAPER

View Article Online
View Journal | View Issue

Cite this: *Phys. Chem. Chem. Phys.*, 2013, **15**, 16828

Supercritically exfoliated ultrathin vanadium pentoxide nanosheets with high rate capability for lithium batteries†

Qinyou An,‡[a] Qiulong Wei,‡[a] Liqiang Mai,*[a] Jiayang Fei,[b] Xu Xu,[a] Yunlong Zhao,[a] Mengyu Yan,[a] Pengfei Zhang[a] and Shizhe Huang[a]

Received 24th June 2013,
Accepted 31st July 2013

DOI: 10.1039/c3cp52624k

www.rsc.org/pccp

Ultrathin V_2O_5 nanosheets were successfully prepared through supercritical solvothermal reaction followed by annealing treatment. The formation of ultrathin nanosheets is owing to Ostwald ripening and the effect of supercritical fluids. As cathode material for lithium batteries, the ultrathin V_2O_5 nanosheets exhibit a capacity of 108 mA h g^{-1} at a high rate of up to 10 C at 2.4–4 V and excellent cyclability with little capacity loss after 200 cycles. The enhanced rate performance is attributed to the shortened diffusion distance and the increased electrode–electrolyte contact area of the ultrathin nanosheet structure. It is also demonstrated that the supercritical solvothermal method is effective and facile to scalably synthesize ultrathin nanomaterials for lithium batteries.

Introduction

Rechargeable lithium batteries (LBs) are attracting great interest for application in powering electric vehicles (EVs) and hybrid electric vehicles (HEVs) owing to their high energy density and long lifespan.[1–4] Rate capability, cyclability, and power density are considered as the three important factors that need to be further improved before their widespread use.[5–7] Designing electrode materials within the nanoscale has become one of the most effective methods to shorten the Li-ion diffusion distance during the charge–discharge process and increase the interfacial contact area between the electrode and the electrolyte, leading to significantly enhanced specific power density and energy density compared with bulk materials.[8–13] Two-dimensional (2D) nanomaterials have been receiving great attention owing to their unique mechanical, electrical, and chemical properties.[14,15] Especially, ultrathin 2D nanosheets (NSs) with atomic-scale thickness have structural advantages in the reversible Li storage process, such as graphene,[16] FeS,[17] SnO_2,[18] and Li_2MSiO_4 (M = Fe, Mn).[19] The development of layered structure metal oxide ultrathin NSs is pursued intensively on the basis of fundamental scientific interest coupled with their widespread application in LBs.

As a cathode material for rechargeable LBs, V_2O_5 delivers a high theoretical capacity of 440 mA h g^{-1} based on the intercalation of three Li ions.[20,21] However, the development of V_2O_5 electrodes was limited by their poor structural stability,[22] low electronic conductivity[23] and poor electrochemical kinetics.[24] Nanostructured vanadium oxides have been widely explored to enhance the electrochemical kinetics. Recently, nanoparticles,[25] nanorods,[26] nanowires,[27] nanotubes,[28] nanobelts,[29] and nanocomposites[30] have been successfully synthesized by a variety of methods and their rate capabilities were improved. Nevertheless, it still remains a big challenge to obtain long-term cycling stability during subsequent rapid lithium insertion–extraction processes. Furthermore, it is important to improve the reversible capacity at high potentials (above 3 V), which is related to high energy density.

As a new kind of reaction medium, supercritical fluids (SCFs) possess unique properties including gas-like diffusivity, low viscosity, and a density closer to that of liquid than gas.[31,32] The surface tension of SCFs completely vanishes above the critical point of the fluids, which is of particular utility in controlling the surface and interface chemistry of materials. Compared with common chemical vapor deposition (CVD) and ultrasonic exfoliation methods, the features of SCFs make the SCF-based solvothermal method as another important approach to synthesize layered crystals with high yield. Recently, Rangappa and

[a] *State Key Laboratory of Advanced Technology for Materials Synthesis and Processing, WUT-Harvard Joint Nano Key Laboratory, Wuhan University of Technology, Wuhan, 430070, P. R. China. E-mail: mlq518@whut.edu.cn; Fax: +86-27-87644867; Tel: +86-27-87467595*

[b] *Department of Materials Science and Engineering, University of Pennsylvania, Philadelphia, Pennsylvania 19104, USA*

† Electronic supplementary information (ESI) available: SEM images of the V_2O_5 microspheres, the V_2O_5 ethanol-gels and the products synthesized by 10 h solvothermal reaction; energy dispersive X-ray spectrometry mapping of the V_2O_5 microflowers; charge–discharge curves and the cycling performance of the ultrathin V_2O_5 nanosheets and amorphous vanadium oxide ultrathin nanosheets in the potential range from 1.5 to 4 V; AC impedance plots of ultrathin V_2O_5 nanosheet and V_2O_5 microsphere cathodes. See DOI: 10.1039/c3cp52624k

‡ Qinyou An and Qiulong Wei contributed equally to this work.

his co-workers successfully employed this process for the preparation of exfoliated graphene nanosheets and for the synthesis of ultrathin Li_2MSiO_4 (M = Fe, Mn) nanosheets with excellent electrochemical performance for LBs.[19] However, the use of SCF-based solvothermal methods to design and synthesize layered V_2O_5 and other nanomaterials is greatly unexplored. In the present work, based on the Ostwald ripening and SCFs exfoliation mechanism, we described a facile and mass-produced route to synthesize ultrathin V_2O_5 NSs with excellent high-rate and long-life performance to serve as the cathode material in rechargeable LBs.

Experimental section

Sample preparation

The preparation of the ultrathin V_2O_5 NSs included two steps. The first step was the preparation of the V_2O_5 gel. V_2O_5 powder (0.51 g) was slowly dissolved in hydrogen peroxide solution (50 mL, 30%) under stirring at room temperature until clear orange solution formed. After stirring for another 15 min and aging for 2 days at room temperature, the solution gradually turned into a dark red V_2O_5 gel. The resulting gel was transferred into a funnel and washed with ethanol five times. Then it was immersed in ethanol for 7 days and a jelly-like precursor finally formed. In the second step, the precursor was transferred into a Teflon-lined autoclave, filled with ethanol up to 80% of the total volume. The autoclave with a stainless steel shell was kept at 250 °C for 12 h and cooled to room temperature naturally. The final product was washed with ethanol three times and then dried at 80 °C for 12 h. Finally the as-obtained products were thermally treated at 400 °C for 2 h in air to form the ultrathin V_2O_5 nanosheets. The atomic force microscopic (AFM) observation was achieved using Bruker MultiMode 8 Atomic Force Microscope.

Material characterization

X-ray diffraction (XRD) measurements were performed to obtain the crystallographic information using a D8 Advance X-ray diffractometer with a non-monochromated Cu Kα X-ray source. Field emission scanning electron microscopic (FESEM) images were collected using a JEOL JSM-7100F. Transmission electron microscopic (TEM) and high-resolution TEM (HRTEM) images were recorded using a JEOL JEM-2100F STEM/EDS microscope.

Electrochemical measurements

The electrochemical measurements were carried out by assembly of 2025 coin cells in a glove box filled with pure argon gas, using lithium discs as both the counter electrode and the reference electrode, and 1 M $LiPF_6$ in a mixture of ethylene carbon/dimethyl carbonate (1 : 1 w/w) as electrolyte. Cathodes were obtained with 70% active material, 20% acetylene black and 10% poly(tetrafluoroethylene). Galvanostatic charge–discharge tests were performed using a multichannel battery testing system (LAND CT2001A). Cyclic voltammetry (CV) and electrochemical impedance spectra (EIS) were recorded on an electrochemical workstation (Autolab PGSTAT 302).

Results and discussion

Time-dependent experiments were carried out to understand the formation process of the ultrathin nanosheets under supercritical solvothermal treatment at 250 °C. Fig. 1 shows the FESEM images of the as-synthesized products obtained at different reaction durations. At the early stage of the reaction (1.5 h), some thick NSs were formed and aggregated to form irregular nanoflowers (Fig. 1a). Upon increasing the reaction time to 3 h, more NSs self-assembled to form uniform nanoflowers of ~200 nm in size (Fig. 1b). Interestingly, with the duration increasing to 4.5 h, NSs grew large along with their thickness decreasing, and some NSs separated from the nanoflowers (Fig. 1c). After increasing the time to 6 h, they self-assembled to uniform microflowers of 1–2 μm (Fig. 1d). After 10 h reaction time (Fig. S1, ESI†), it was clearly found that the microflowers became irregular with fewer nanosheets than before, and large nanosheets were scattered around the large microflowers. Finally, with the rapid growth of NSs to larger and larger ones, they were exfoliated from the microflowers after 12 h (Fig. 1e), which exhibited a width of ~1 μm and smooth surfaces. The high-magnification SEM image (Fig. 1e, inset) shows that the thickness of NSs is below 10 nm. After annealing the ultrathin NSs at 400 °C in air (Fig. 1f), their morphology remained the same, but with rough surfaces (Fig. 1f, inset). As a control experiment, after annealing the solvothermally prepared microflowers (duration 6 h, Fig. 1d), agglomerated V_2O_5 microspheres are obtained (Fig. S2, ESI†). The crystal structure of the ultrathin

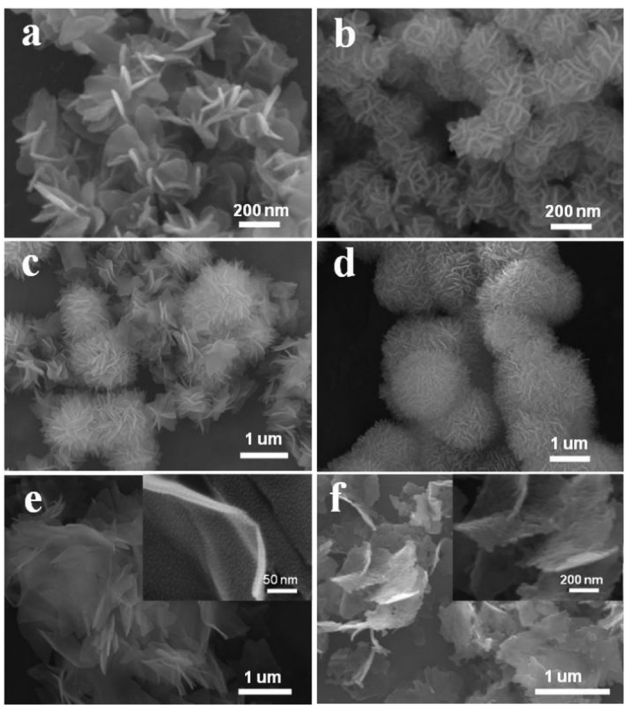

Fig. 1 SEM images of the products synthesized under different solvothermal times: (a) 1.5 h, (b) 3 h, (c) 4.5 h, (d) 6 h, and (e) 12 h. (f) Ultrathin V_2O_5 nanosheets obtained by annealing solvothermally prepared ultrathin nanosheets (e) in air at 400 °C.

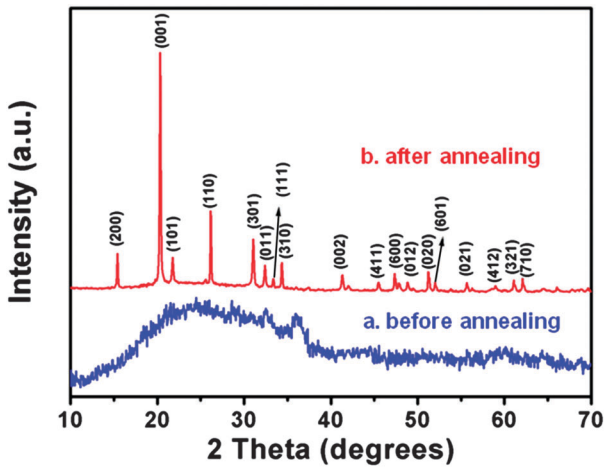

Fig. 2 X-ray diffraction patterns of ultrathin vanadium oxide nanosheets before and after annealing.

NSs before and after annealing was determined by XRD (Fig. 2). Before annealing, there are no obvious peaks assigned to crystalline vanadium oxides, which indicates that the ultrathin vanadium oxide NSs obtained by the solvothermal process are amorphous. After annealing, the ultrathin NSs were well crystallized. All the diffraction peaks are indexed and assigned to the orthorhombic V_2O_5 phase (JCPDS card no. 00-041-1426, space group: *Pmmm* (59), a = 11.516 Å, b = 3.566 Å, c = 3.777 Å).

Representative TEM images and HRTEM images show that the solvothermally synthesized ultrathin NSs (Fig. 3a and b) have smooth surfaces and are amorphous. TEM images of the ultrathin NSs (Fig. 3c) show that the large V_2O_5 NSs contain many smaller nanosheets with different sizes. The high-resolution transmission electron microscopic (HRTEM) images (Fig. 3d) were taken from the centre of nanosheets. The lattice fringes are clearly visible with spacings of 3.40 and 2.61 Å, corresponding to the *d*-spacings of the (110) and (310) planes of orthorhombic V_2O_5, respectively. This indicates that the V_2O_5 crystal structural layers were stacked along [00l], which is consistent with the XRD results (Fig. 2). The FFT analysis pattern (inset of Fig. 3d) reveals the single-crystalline nature of the V_2O_5 nanosheets. Atomic force microscopy (AFM) was used to determine the thickness of the ultrathin V_2O_5 NSs (Fig. 4). Multiple cross-sectional views of the sample laid on a Si substrate were recorded, and a number of step heights were measured across the sample. The step height profiles show that the thickness of ultrathin V_2O_5 NSs is ~6 nm, which indicates that the individual NSs are a few layers thick.

A plausible schematic illustration for the formation mechanism of the ultrathin V_2O_5 NSs is proposed in Fig. 4. Firstly, V_2O_5 gels prepared by the sol–gel method are employed as the precursor. V_2O_5 gels have typical layered structure and could serve as versatile hosts for ionic and organic molecular species to intercalate.[33] Water molecules are intercalated between the layers of the gels during their formation. After being washed with ethanol and soaked in ethanol for aging for one week, the water molecules are gradually replaced by ethanol to form V_2O_5 ethanol-gels,

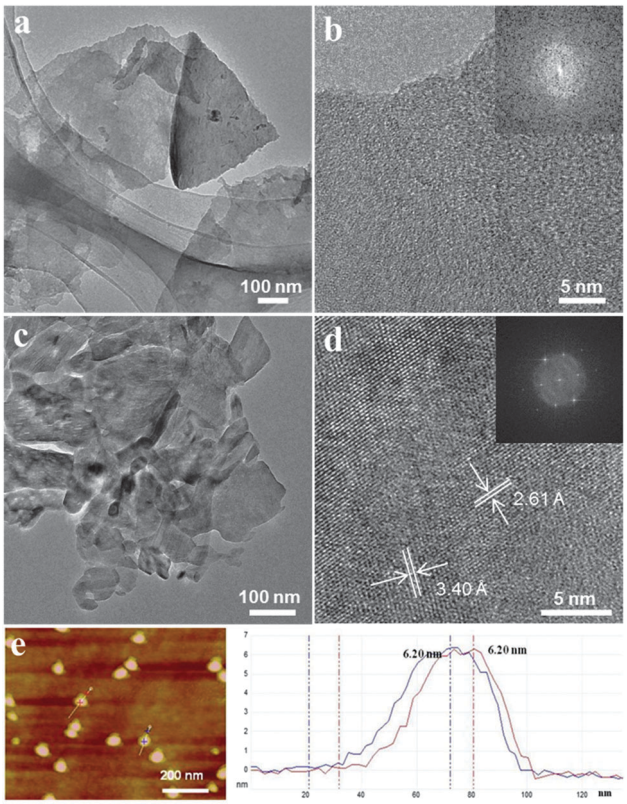

Fig. 3 TEM and HRTEM images of the ultrathin nanosheets: (a, b) before and (c, d) after annealing, respectively; inset of (d) FFT patterns of the ultrathin V_2O_5 nanosheets. (e) AFM images and height profiles of ultrathin V_2O_5 NSs.

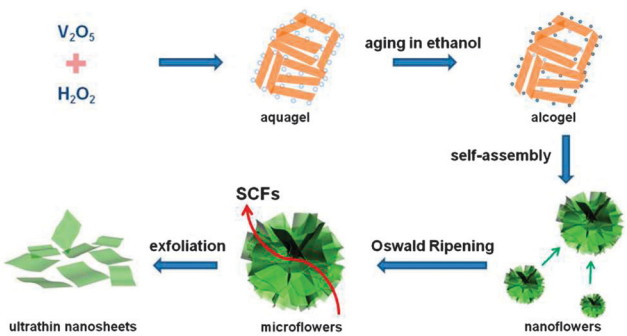

Fig. 4 Schematic illustration of the procedure for fabricating the ultrathin vanadium oxide nanosheets.

which consists of reticular layers (Fig. S3, ESI†). The reticular layered V_2O_5 ethanol-gels are flaked by supercritical medium, and self-assemble to form flower-like spheres. As the reaction progressed, the sizes of flower-like spheres rapidly increase (Fig. 1b–d), which is the result of Ostwald ripening.[36–39] This indicates the solution growth of larger crystals from those of smaller size. To lower the total energy of the SCF system, the molecules of small nanoflowers diffuse and recrystallize on the surfaces of larger nanoflowers. Thus, the larger nanoflowers grow to microflowers and smaller ones are totally consumed. At last, the grown ultrathin NSs are exfoliated from the microflowers.

This exfoliation process is owing to the unique features of the SCFs, *e.g.* low interfacial tension, excellent wetting of surfaces and high diffusion coefficients.[19,34,35] These features allow supercritical solvents to rapidly penetrate all the interior of microflower and vanadium oxide layers with high diffusivity, and then to exfoliate the vanadium oxide NSs down to a few layers. Energy dispersive X-ray spectrometry (EDS) mapping was performed to confirm that the supercritical solvents (ethanol) penetrated into the microflowers' NSs (Fig. S4, ESI†). Carbon atoms are homogeneously distributed in all of the NSs, which come from the ethanol. These results indicate that SCFs form a homogeneous phase with gas or organic compounds in solvothermal systems, providing a unique reaction medium for preparing organic–inorganic hybrid nanostructures, which traditional hydrothermal methods could not provide.[19] After annealing treatment, the exfoliated NSs' morphology remained the same. However, the microflowers agglomerated after annealing and formed V_2O_5 microspheres (Fig. S2, ESI†), because the mass transfer is faster than the separation of the NSs during the heat treatment.

Coin cells with metallic lithium as an anode were assembled to investigate the enhanced electrochemical performance of the ultrathin V_2O_5 NS cathodes. Cyclic voltammogram (CV) of the ultrathin V_2O_5 NSs was measured at a scan rate of 0.1 mV s^{-1} in the potential range from 2.4 to 4.0 V (Fig. 5a). The cathodic and anodic peaks are ascribed to the lithium ion insertion and extraction, respectively. Two main cathodic peaks appear at potentials of 3.4 and 3.1 V, corresponding to the phase transformations from α-V_2O_5 to ε-$Li_{0.5}V_2O_5$ and δ-LiV_2O_5, the processes of which are expressed in eqn (1) and (2),[40–42] respectively.

$$V_2O_5 + 0.5Li^+ + 0.5e^- = \varepsilon\text{-}Li_{0.5}V_2O_5 \quad (1)$$

$$\varepsilon\text{-}Li_{0.5}V_2O_5 + 0.5Li^+ + 0.5e^- = \delta\text{-}LiV_2O_5 \quad (2)$$

In the subsequent scans, the shapes of the curves are almost identical, which indicates good reversibility of the lithium insertion process above 3 V.[43,44]

The cycling performance was further evaluated by galvanostatic discharge–charge testing. As shown in Fig. 5b, the initial discharge capacity of both ultrathin V_2O_5 NSs and V_2O_5 microspheres is 146 mA h g^{-1} at 1 C (1 C is equivalent to 147 mA g^{-1}), very close to the theoretical value of 147 mA h g^{-1} for the formation of δ-LiV_2O_5. And this value is higher than that of the V_2O_5 thin films (142 mA h g^{-1}) reported by Wang *et al.*[45] and the hierarchical V_2O_5 hollow microspheres (144 mA h g^{-1}) reported by Pan *et al.*[46] After 50 cycles (Fig. 5b), their discharge capacities of 140 and 136 mA h g^{-1} still remained the same, corresponding to 95.9% and 93.2% of the initial capacity, respectively. The coulombic efficiency is close to 100% throughout the cycling test. When the voltage range is extended to 1.5–4 V (Fig. S5, ESI†), the capacity increases to 358 mA h g^{-1}, because of the intercalation of more Li^+ ions, however the cycling stability is not as good as that at 2.4–4.0 V, due to the irreversible formation of ω-$Li_3V_2O_5$.[40–43] The electrochemical performance of amorphous ultrathin NSs was also measured (Fig. S6, ESI†). There are no plateaus during charge–discharge and capacity fades fast, associated with their poor crystallinity.

For the applications of LBs in EVs and HEVs, both good rate capability and excellent cyclability are necessary.[47,48] To evaluate the rate capability, the ultrathin V_2O_5 NS cathodes were cycled at various rates, ranging from 1 to 15 C (Fig. 5c). As the rate increases from 1 to 15 C, the discharge capacity of ultrathin V_2O_5 NS cathodes decreases gradually from 146 to 100 mA h g^{-1}. After the high rate measurement, when the rate is reduced back to 1 C, a discharge capacity of 136 mA h g^{-1} can be recovered. However, the V_2O_5 microsphere cathode exhibits a similar capacity to the ultrathin nanosheet cathodes at the 1 C rate, but its capacity decreases to ~40 mA h g^{-1} at 15 C. These results

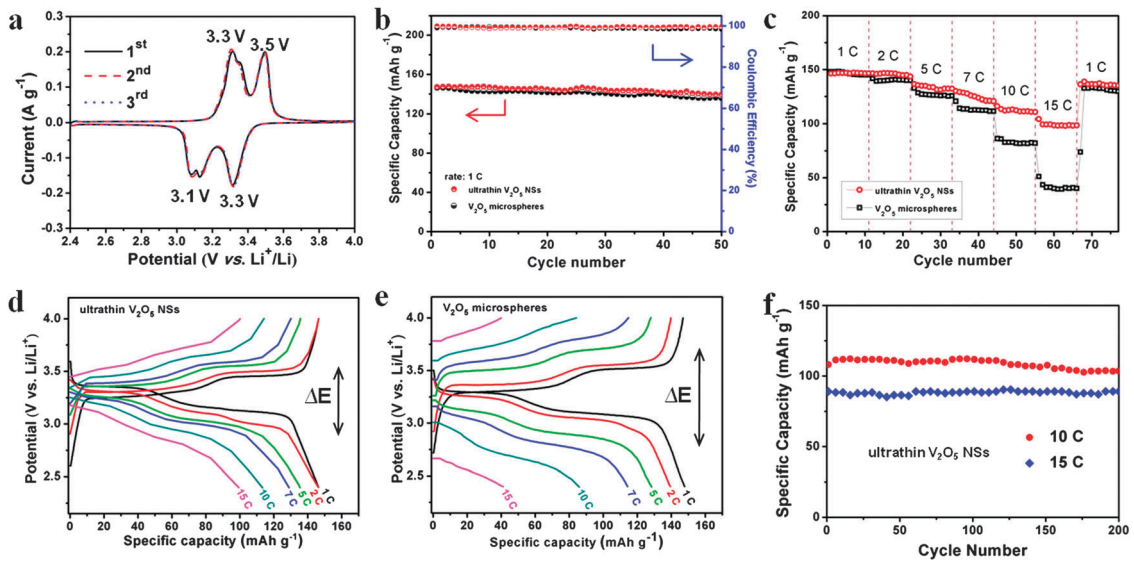

Fig. 5 (a) Cyclic voltammograms at a scan rate of 0.1 mV s^{-1}; (b) cycling performance of ultrathin V_2O_5 NS and V_2O_5 microsphere cathodes recorded at a rate of 1 C; (c) rate performance, the corresponding charge–discharge curves of (d) ultrathin V_2O_5 NS and (e) V_2O_5 microsphere cathodes at various rates from 1 C to 15 C. (f) Cycling performance of the ultrathin V_2O_5 NS cathodes at high rates of 10 C and 15 C.

indicate the excellent rate capability and structural stability of ultrathin V_2O_5 NSs. Two voltage plateaus are clearly observed even at a high rate in charge and discharge curves (Fig. 5d and e), which is quite consistent with the CV curves. The overpotential of the ultrathin V_2O_5 NS cathodes is smaller than that of the V_2O_5 microspheres, which indicates the faster ion diffusion and higher reversibility of NS cathodes.[48] The electrochemical impedance spectra (EIS) were used to provide further insights (Fig. S7, ESI†). The Nyquist plots indicate that the charge transfer resistance (R_{ct}) of the ultrathin V_2O_5 NS cathode is much lower than the microsphere cathode, which is consistent with the overpotential values. Moreover, the cycling performance of the ultrathin V_2O_5 NS cathodes at high rates of 10 C and 15 C were tested (Fig. 5f). The initial specific discharge capacities were 108 and 90 mA h g^{-1} at the rates of 10 and 15 C, respectively. Remarkably, their capacities were retained at 104 and 90 mA h g^{-1} after 200 cycles, corresponding to 96.2% and 100% of their initial capacity, respectively. The electrochemical performance of the ultrathin V_2O_5 NSs is good compared to those of many published V_2O_5 electrodes, in terms of high-rate capability and cycling performance (Table S1, ESI†).

The enhanced electrochemical performance of V_2O_5 NS electrodes depends on not only the good crystallinity of V_2O_5, but also the designed ultrathin nanosheet structure. The solid-state diffusion time of lithium over ultrathin V_2O_5 NSs was estimated based on the formula $t = L^2/D$, where D is the Li^+ diffusion coefficient for bulk V_2O_5 ($D_{Li} = 10^{-12}$ cm^2 s^{-1}),[49] and the diffusion time for the Li^+ into the V_2O_5 layer ($L \approx 6$ nm) was about 0.36 s. This means that the high utilization of V_2O_5 even under rapid ion diffusion results in the outstanding high-rate capability. Meanwhile, the decreased thickness of NSs reduces the charge transfer resistance and the overpotentials (Fig. S7, ESI,† Fig. 5d and e). Moreover, the ultrathin V_2O_5 NSs could effectively relax the mechanical strain generated during charge–discharge.[19]

Conclusions

Ultrathin V_2O_5 NSs have been prepared by a supercritical solvothermal method followed by annealing at 400 °C in air. The morphology of the NSs is controlled by adjusting the solvothermal time. As a potential cathode material for lithium batteries, the ultrathin V_2O_5 NS cathode displays high reversible capacity, low capacity loss and high coulombic efficiency. Especially, it shows high-rate and long-life capability with initial capacity of up to 90 mA h g^{-1} at 15 C and 100% capacity retention after 200 cycles. The excellent rate capability is ascribed to the ultrathin 2D nanostructure that facilitates Li-ion diffusion in the electrode. Furthermore, the novel SCF solvothermal approach provides an effective strategy to synthesize ultrathin nanomaterials.

Acknowledgements

This work was supported by the National Natural Science Foundation of China (51072153, 51272197), the Program for New Century Excellent Talents in University (NCET-10-0661), the National Basic Research Program of China (2013CB934103, 2012CB933003) and the Fundamental Research Funds for the Central Universities (2012-II-001, 2013-YB-001). Thanks to Prof. C. M. Lieber of Harvard University, Prof. Dongyuan Zhao of Fundan University and Dr Jun Liu of Pacific Northwest National Laboratory for strong support and stimulating discussions.

Notes and references

1 J.-M. Tarascon and M. Armand, *Nature*, 2001, **414**, 359.
2 B. Kang and G. Ceder, *Nature*, 2009, **458**, 190.
3 B. Dunn, H. Kamath and J.-M. Tarascon, *Science*, 2011, **334**, 928.
4 H. Wu, G. Chan, J. W. Choi, I. Ryu, Y. Yao, M. T. McDowell, S. W. Lee, A. Jackson, Y. Yang and L. Hu, *Nat. Nanotechnol.*, 2012, **7**, 310.
5 H. Zhang, X. Yu and P. V. Braun, *Nat. Nanotechnol.*, 2011, **6**, 277.
6 J. Y. Huang, L. Zhong, C. M. Wang, J. P. Sullivan, W. Xu, L. Q. Zhang, S. X. Mao, N. S. Hudak, X. H. Liu and A. Subramanian, *Science*, 2010, **330**, 1515.
7 H. G. Jung, M. W. Jang, J. Hassoun, Y. K. Sun and B. Scrosati, *Nat. Commun.*, 2011, **2**, 516.
8 Y. Wang, K. Takahashi, K. H. Lee and G. Cao, *Adv. Funct. Mater.*, 2006, **16**, 1133.
9 M. G. Kim and J. Cho, *Adv. Funct. Mater.*, 2009, **19**, 1497.
10 Y. S. Hu, X. Liu, J. O. Müller, R. Schlögl, J. Maier and D. S. Su, *Angew. Chem., Int. Ed.*, 2009, **48**, 210.
11 P. G. Bruce, B. Scrosati and J. M. Tarascon, *Angew. Chem., Int. Ed.*, 2008, **47**, 2930.
12 Y. Shi, B. Guo, S. A. Corr, Q. Shi, Y. S. Hu, K. R. Heier, L. Chen, R. Seshadri and G. D. Stucky, *Nano Lett.*, 2009, **9**, 4215.
13 C. Han, Y. Pi, Q. An, L. Mai, J. Xie, X. Xu, L. Xu, Y. Zhao, C. Niu and A. M. Khan, *Nano Lett.*, 2012, **12**, 4668.
14 (*a*) H. Ji, L. Zhang, M. T. Pettes, H. Li, S. Chen, L. Shi, R. Piner and R. S. Ruoff, *Nano Lett.*, 2012, **12**, 2446; (*b*) Z. Wang, D. Xu, L. Wang and X. Zhang, *ChemPlusChem*, 2012, **77**, 124.
15 (*a*) X. Zhao, L. Zhang, S. Murali, M. D. Stoller, Q. Zhang, Y. Zhu and R. S. Ruoff, *ACS Nano*, 2012, **6**, 5404; (*b*) X. Rui, Z. Lu, H. Yu, D. Yang, H. H. Hng, T. M. Lim and Q. Yan, *Nanoscale*, 2013, **5**, 556.
16 G. Wang, B. Wang, X. Wang, J. Park, S. Dou, H. Ahn and K. Kim, *J. Mater. Chem.*, 2009, **19**, 8378.
17 C. Xu, Y. Zeng, X. Rui, N. Xiao, J. Zhu, W. Zhang, J. Chen, W. Liu, H. Tan and H. H. Hng, *ACS Nano*, 2012, **6**, 4713.
18 C. Wang, G. Du, K. Ståhl, H. Huang, Y. Zhong and J. Jiang, *J. Phys. Chem. C*, 2012, **116**, 4000.
19 (*a*) D. Rangappa, K. D. Murukanahally, T. Tomai, A. Unemoto and I. Honma, *Nano Lett.*, 2012, **12**, 1146; (*b*) D. Rangappa, K. Sone, M. Wang, U. K. Gautam, D. Golberg, H. Itoh, M. Ichihara and I. Honma, *Chem.–Eur. J.*, 2010, **16**, 6488.
20 (*a*) M. S. Whittingham, Y. N. Song, S. Lutta, P. Y. Zavalij and N. A. Chernova, *J. Mater. Chem.*, 2005, **15**, 3362; (*b*) H. C. Pang, P. Cheng, H. B. Yang, J. L. Lu, C. X. Guo, G. L. Ning and C. M. Li, *Chem. Commun.*, 2013, **49**, 1536.

21 A. Pan, J. G. Zhang, Z. Nie, G. Cao, B. W. Arey, G. Li, S. Q. Liang and J. Liu, *J. Mater. Chem.*, 2010, **20**, 9193.
22 C. Ban, N. A. Chernova and M. S. Whittingham, *Electrochem. Commun.*, 2009, **11**, 522.
23 J. Muster, G. T. Kim, V. Krstić, J. G. Park, Y. W. Park, S. Roth and M. Burghard, *Adv. Mater.*, 2000, **12**, 420.
24 T. Watanabe, Y. Ikeda, T. Ono, M. Hibino, M. Hosoda, K. Sakai and T. Kudo, *Solid State Ionics*, 2002, **151**, 313.
25 S. H. Ng, T. J. Patey, R. Büchel, F. Krumeich, J.-Z. Wang, H.-K. Liu, S. E. Pratsinis and P. Novák, *Phys. Chem. Chem. Phys.*, 2009, **11**, 3748.
26 K. Takahashi, S. J. Lim, Y. Wang and G. Z. Cao, *Jpn. J. Appl. Phys., Part 1*, 2005, **44**, 662.
27 L. Q. Mai, X. Xu, L. Xu, C. H. Han and Y. Z. Luo, *J. Mater. Res.*, 2011, **26**, 2175.
28 Y. Wang, K. Takahashi, H. M. Shang and G. Z. Cao, *J. Phys. Chem. B*, 2005, **109**, 3085.
29 H. Wang, K. Huang, C. Huang, S. Liu, Y. Ren and X. Huang, *J. Power Sources*, 2011, **196**, 5645.
30 X. F. Zhang, K.-X. Wang, X. Wei and J.-S. Chen, *Chem. Mater.*, 2011, **23**, 5290.
31 T. Adschiri, Y. Hakuta and K. Arai, *Ind. Eng. Chem. Res.*, 2000, **39**, 4901.
32 K. J. Ziegler, R. C. Doty, K. P. Johnston and B. A. Korgel, *J. Am. Chem. Soc.*, 2001, **123**, 7797.
33 J. Livage, *Chem. Mater.*, 1991, **3**, 578.
34 D. Rangappa, K. Sone, M. Wang, U. K. Gautam, D. Golberg, H. Itoh, M. Ichihara and I. Honma, *Chem.–Eur. J.*, 2010, **16**, 6488.
35 K. P. Johnston and P. S. Shah, *Science*, 2004, **303**, 482.
36 Y. Zhao and L. Jiang, *Adv. Mater.*, 2009, **21**, 3621.
37 J. Li and H. C. Zeng, *J. Am. Chem. Soc.*, 2007, **129**, 15839.
38 B. Liu and H. C. Zeng, *Small*, 2005, **1**, 566.
39 H. G. Yang and H. C. Zeng, *J. Phys. Chem. B*, 2004, **108**, 3492.
40 A. M. Cao, J. S. Hu, H. P. Liang and L. J. Wan, *Angew. Chem., Int. Ed.*, 2005, **44**, 4391.
41 L. Q. Mai, L. Xu, C. H. Han, X. Xu, Y. Z. Luo, S. Y. Zhao and Y. L. Zhao, *Nano Lett.*, 2010, **10**, 4750.
42 H. Groult, K. Le Van, A. Mantoux, L. Perrigaud and P. Doppelt, *J. Power Sources*, 2007, **174**, 312.
43 T. Zhai, H. Liu, H. Li, X. Fang, M. Liao, L. Li, H. Zhou, Y. Koide, Y. Bando and D. Golberg, *Adv. Mater.*, 2010, **22**, 2547.
44 X. F. Zhang, K. X. Wang, X. Wei and J. S. Chen, *Chem. Mater.*, 2011, **23**, 5290.
45 S. Wang, S. Li, Y. Sun, X. Feng and C. Chen, *Energy Environ. Sci.*, 2011, **4**, 2854.
46 A. Pan, T. Zhu, H. B. Wu and X. W. D. Lou, *Chem.–Eur. J.*, 2013, **19**, 494.
47 J. Liu, H. Xia, D. Xue and L. Lu, *J. Am. Chem. Soc.*, 2009, **131**, 12086.
48 L. Q. Mai, Q. L. Wei, Q. Y. An, X. C. Tian, Y. L. Zhao, X. Xu, L. Xu, L. Chang and Q. J. Zhang, *Adv. Mater.*, 2013, **25**, 2969.
49 J. Yan, A. Sumboja, E. Khoo and P. S. Lee, *Adv. Mater.*, 2011, **23**, 746.